RSC Advances

ROYAL SOCIETY OF CHEMISTRY

www.rsc.org/advances

Cite this: DOI: 10.1039/c0xx00000x

www.rsc.org/xxxxxx

ARTICLE TYPE

High specific surface area $LaMO_3$ (M=Co, Mn) hollow spheres: synthesis, characterization and catalytic properties in methane combustion

Guangsheng Guo, Kuo Lian, Lijuan Wang, Fubo Gu*, Dongmei Han, Zhihua Wang*

Received (in XXX, XXX) Xth XXXXXXXXX 20XX, Accepted Xth XXXXXXXXX 20XX
DOI: 10.1039/b000000x

Perovskite-type metal oxides have been regarded as promising materials for solar cells and catalysts. However, they suffer from a major challenge on low specific surface area. In this work, high specific surface area $LaMO_3$ (M=Co, Mn) hollow spheres were synthesized by a hard template method. The influence of the reactant ratios on the properties of the products was investigated. The formation of La_2O_3, Co_3O_4 or MnO_2 prevented the growth of $LaMO_3$, which resulted in the variations of the composition, morphology, specific surface area, surface chemistry and catalytic activity of the products. Acid washing process could remove La_2O_3 and Co_3O_4, which led to the enhancement of the specific surface area of $LaCoO_3$. Due to the high reactant concentration and the slow heating rate, multishelled $LaMnO_3$ hollow spheres with a high specific surface area of 42.6 m^2/g were formed, which showed the best catalytic activity in methane combustion.

1. Introduction

Perovskite-type metal oxides have been regarded as promising materials for solar cells and catalysts.[1-4] However, they suffer from a major challenge on low specific surface area.[5] For example, highly crystalline $LaCoO_3$ with a low specific surface area of 11 m^2/g was prepared by co-precipitation method.[6] $LaFe_{0.94}Pd_{0.06}O_3$ with a specific surface area of 23.5 m^2/g was prepared through the classical citrate complexation procedure.[7] By sol-gel method, $LaMO_3$ (M=Mn and Co) with specific surface areas of 17.5 to 23.5 m^2/g were synthesized.[8-9] Therefore, it is highly desirable to develop an effective strategy for synthesis of high specific surface area perovskites. Recently, three dimensionally ordered macroporous $LaFeO_3$ with a high specific surface area of 32 m^2/g was prepared, which exhibited excellent activity for catalytic oxidation of soot.[10-11]

Hollow materials with low density and high specific surface area have attracted much attention. Template-directed route has been considered as an effective strategy to synthesize hollow materials. Diverse hollow spheres, such as Co_3O_4, TiO_2, WO_3, In_2O_3 and Eu^{3+}-doped Y_2O_3 with high specific surface areas have been synthesized by carbon sphere template method.[12-16] However, perovskite-type hollow spheres have rarely been reported.

In this work, high specific surface area $LaMO_3$ (M=Co, Mn) hollow spheres were synthesized by carbon sphere template method. The effects of reactant ratio on the composition, morphology, specific surface area and surface chemistry of the products were investigated. Acid washing process was used to further enhance the specific surface areas of the products.[17-18] In addition, catalytic combustion of methane has several advantages compared to the conventional combustion, such as low temperature and high efficiency, which effectively abates thermal NOx formation.[19] The performance of the synthesized $LaMO_3$ (M=Co, Mn) hollow spheres in the catalytic combustion of methane was evaluated.

2. Experimental section

2.1. Synthesis of $LaMO_3$ (M=Co, Mn) hollow spheres

The template of carbon sphere had a diameter of 600-800 nm (Fig. S1) which were synthesized by hydrothermal method.[20] In a typical preparation procedure, 8.0 g glucose was dissolved in 70 mL deionized water under vigorous stirring, and then sealed in a 100 mL Teflon-lined autoclave at 180 °C for 6 h. The products were obtained by centrifugation, washing with deionized water and alcohol, and then dried in an oven at 80 °C for 12 h.

A typical preparation procedure for $LaCoO_3$ hollow sphere was as follows: firstly, a certain amount of $La(NO_3)_3 \cdot 6H_2O$ and $Co(NO_3)_2 \cdot 6H_2O$ were dissolved in 40 mL deionized water. The ion concentration of lanthanum was 0.5 M. The molar ratio of lanthanum and cobalt was 1:1, 1:1.5, 1:2, 1:3 and 1:5. Secondly, carbon spheres (0.2 g) were dispersed in the nitrate solution with ultrasonicating for 30 min, and then sealed in a 100 mL Teflon-lined autoclave at 180 °C for 6 h. The precursors were obtained by centrifugation, washing with distilled water and ethanol for three cycles, and then dried in an oven at 80 °C for 12 h. Finally, the $LaCoO_3$ precursors were calcined at a ramp of 5 °C /min from RT to 400 °C and then kept at 400 °C for 2 h, and then at a ramp of 5 °C /min from 400 °C to 700 °C for 4 h in air. The obtained products were washed with 0.2 M acetic acid with vigorous

stirring for 60 min. Then the products were washed with distilled water, centrifuged and dried. The samples obtained with the reactant ratios of 1:1, 1:1.5, 1:2, 1:3, 1:5 of lanthanum and cobalt were denoted as LC-1, LC-1.5, LC-2, LC-3, LC-5. The corresponding acid washing samples were denoted as WLC-1, WLC-1.5, WLC-2, WLC-3, WLC-5, respectively.

For the synthesis of $LaMnO_3$, a certain amount of $La(NO_3)_3 \cdot 6H_2O$ and $Mn(NO_3)_2$ (50 wt% aqueous solution) were dissolved in 40 mL deionized water. The ion concentration of lanthanum was 1 M. The reactant ratios of lanthanum and manganese were 1:1, 1:2, 1:3, 1:4, 1:5 and 1:6. Carbon spheres (0.2 g) were dispersed in the nitrate solution with ultrasonicating for 30 min, and then sealed in a 100 mL Teflon-lined autoclave at 180 ^oC for 6 h. The precursors were obtained by centrifugation, washing with deionized water, and then dried in an oven at 80 ^oC for 12 h. The obtained $LaMnO_3$ precursors were calcined in two steps: (i) firstly, calcinated in a N_2 flow of 50 mL/min at a ramp of 1 °C /min from RT to 300 °C, and then kept at 300 °C for 3 h. Finally, cooled to 50 °C in same atmosphere; (ii) the obtained sample was calcinated in an air flow of 50 mL/min at a ramp of 1 ^oC /min from RT to 300 °C, and held at 300 °C for 2 h. Then, calcinated at the same ramp from 300 to 700 °C and maintained at 700 °C for 3 h. The samples obtained with the reactant ratios of 1:1, 1:2, 1:3, 1:5, 1:6 of lanthanum and manganese were denoted as LM-1, LM-2, LM-3, LM-4, LM-5, LM-6, respectively.

The phase composition of the samples was characterized by X-ray diffraction (XRD) performed on D/max2500VB2+/PC X-ray diffractometer using graphite monochromatized Cu Kα radiation (λ = 0.15406 nm). The morphology of the products was observed by Hitachi H-800 transmission electron microscopy (TEM). Energy dispersive X-ray spectromete (EDX) of the samples was recorded on S-4700 scanning electron microscope (SEM) with EDX Octane Super. The Brunauer–Emmett–Teller (BET) specfic surface area was determined using an AutoChem Sorption Analyzer (NOVA-1200). Hydrogen temperature programmed reduction (H2-TPR) was performed using an Automated Catalyst Characterization System (AutoChem II 2920 V3.05, Micromeritics Instrument Corporation). The XPS analysis was performed using a Thermo ESCALAB 250 analyzer. The binding energies for each spectrum were calibrated using a C1s spectrum of 284.6 eV. Fourier transform infrared (FT-IR) spectrum was recorded on a Bruker Vector 22 FT-IR spectrophotometer using a KBr pellet.

2.2. Catalytic activity measurement

Catalytic activities of the $LaMO_3$ (M=Co, Mn) hollow spheres (50 mg) were evaluated on a fixed-bed quartz reactor (di=0.6 cm; l=40 cm) under atmospheric pressure. The total flow rate of the feed gas was 25 mL/min, in which methane was 3.0 vol. %, air was used as balance gas. The weight hourly space velocity (WHSV) of the feed gas was 30,000 mL/($g_{cat} \cdot h$). An on-line gas chromatograph was used to analyze the contents of gases (GC-9790, FULI). The sensitivity to sulfur poisoning was evaluated after exposure to 100 ppm SO_2 at 600 ^oC for 3 h.

3. Results and discussion

3.1. Characterization of $LaMO_3$ (M=Co, Mn) hollow spheres

Fig. 1a-1e show the TEM images of $LaCoO_3$ hollow spheres prepared with different reactant ratios of lanthanum and cobalt. The contrast difference between the dark edge and the pale center in the TEM images provides convincing evidence of the hollow sphere. It can be seen that the diameter of as-prepared $LaCoO_3$ hollow spheres ranges from 100 nm to 300 nm and the shell thickness ranges from 15 nm to 35 nm. In addition, some hollow spheres are broken. When the reactant ratio of lanthanum and cobalt is higher than 5, the hollow structure can't be obtained. In Fig. 1b, broken and unbroken hollow spheres in large scale are observed, which indicates that perovskite-type $LaCoO_3$ hollow spheres are prepared successfully by carbon template method.

The TEM images of the $LaMnO_3$ prepared with the reactant ratios of lanthanum and manganese from 1:3 to 1:6 is shown in Fig.1 (f-i). The LM-5 shows uniform hollow spheres with a diameter of ca. 200 nm, and the thickness of the shells is ca. 20 nm. The size of the hollow spheres (180 nm) is reduced to about 60% of the original size of template spheres. This reduction is mainly due to the shrinkage of template because of further carbonization of organic matters and the densification of the products during the thermal treatment.[21] Comparing with $LaCoO_3$, $LaMnO_3$ shows a multishelled hollow structure (Fig. 1i). The difference is from the programmable heating process. Dong et. al have found low heating rate can result in multishelled ZnO hollow spheres.[22] In this work, the lower heating rate can result in two or three layers of $LaMnO_3$ hollow spheres. Moreover, when the concentration of metal salts is higher, more metal ions can be adsorbed on the surface of carbon spheres, which is helpful to form multishelled structures.

Fig. 2a shows XRD patterns of LC-1, LC-1.5, LC-2, LC-3 and LC-5. LC-1 is composed of $LaCoO_3$ and La_2O_3. The obtained LC-1.5 sample is assigned to perovskite-type $LaCoO_3$ phase (JCPDS PDF# 48-0123), and no impurity peak is found. When the molar ratio of lanthanum and cobalt is higher than 1:1.5, a mixed phase of $LaCoO_3$ and Co_3O_4 is formed. These results indicate that the adsorption ability of the carbon spheres to lanthanum and cobalt ions may be different. The similar results appear in the synthesis of $LaMnO_3$.

Fig. 2b shows the XRD patterns of the as-prepared $LaMnO_3$. By contrasting the standard XRD pattern of $LaMnO_3$ (JCPDS PDF# 82-1152), the diffraction peaks of LM-5 can be indexed to rhombohedral structure. When the molar ratio of lanthanum and manganese is lower than 1:5, La_2O_3 will appear in the products. With the increasing of manganese, the peak intensities of La_2O_3 decrease obviously. In addition, the mean grain sizes of the samples were estimated using the Debye-Scherrer equation. The crystallite size of LM-5 is 16.8 nm, which is much smaller than other $LaMnO_3$,[23-24] suggesting that carbon sphere template method can greatly reduce the crystallite size. The EDX images of LM-1 to LM-6 are shown in Fig S2, which indicate the La/Mn atom ratios of LM-1 to LM-6 are 1:0.37, 1:0.69, 1:0.80, 1:0.90, 1:1.07 and 1:1.35, respectively.

The surface of carbon sphere is hydrophilic with OH^- groups, which can absorb metal ions. $LaMO_3$ hollow spheres are formed by absorption of La^{3+}, Co^{3+} and Mn^{3+} on the carbon spheres due to the electrostatic interaction and coordination with surface hydroxyl groups, and subsequently removed the templates by calcinations. When the molar ratio of lanthanum and manganese is lower than 1: 3, the hollow structure can't be obtained, which

possibly results from the different adsorption ability of carbon spheres to metal ions. From our experiment, the adsorption ability of La^{3+} on the surface of carbon spheres is stronger than that of Co^{3+} and much stronger than Mn^{3+}. When the ratio of La^{3+} and Mn^{3+} is lower than 1:3, more La_2O_3 is formed which prevents the growth of $LaMnO_3$. Therefore, the hollow structure can't be obtained. Moreover, the adsorption ability can be weakened by ion concentration. When Mn^{3+} concentration is relatively high, the adsorption amounts of La^{3+} and Mn^{3+} on the surface of carbon spheres will be close. When the molar ratio of Mn^{3+} and La^{3+} is close to 5, relatively pure $LaMnO_3$ can be obtained.

The nitrogen adsorption-desorption isotherms of $LaMnO_3$ hollow spheres indicate that all these samples show the characteristic of mesoporous structures in Fig. S3. The isotherm of LM-5 can be categorized as type IV with a distinct hysteresis loop, which is the characteristic of mesoporous structure. The pore parameters and specific surface areas of $LaMnO_3$ are summarized in Table 1. The specific surface areas are different between LM-5 and other $LaMnO_3$, demonstrating that the hollow structure is varied by the ratio of lanthanum and manganese. LM-5 has a largest specific surface area of 42.6 m^2/g with a pores size distribution of 10-20 nm (Fig. S3b), and the other samples exhibits lower specific surface areas from 22 to 34 m^2/g. The excess lanthanum or manganese results in the formation of La_2O_3 or Mn_2O_3, which prevents the formation of $LaMnO_3$ hollow spheres, and reduces the specific surface area of the products.

Fig. S4 and Fig. 3(a-b) are the XPS spectra of the as-prepared $LaCoO_3$ samples. As Fig. S4 shown, the LC-1 sample exhibits well-defined doublets for this La 3d core-level. According to the fitting procedure carried out, the main peak for the spin-orbit component[25], at 835.3 eV, can be detected. This contribution implies the presence of La_2O_3 (835.7 eV). [26] The main peak of the LC-1.5 sample can be detected at 834.5 eV, displaces to higher value with respect to that observed in $LaCoO_3$ (833.9 eV), indicative of the contribution of La_2O_3 specie on the surface of catalyst. LC-2, LC-3, LC-5 are observed with binding energies of 833.9 eV, 833.4 eV, 833.7 eV, respectively, indicates that the presence of La^{3+} in $LaCoO_3$ (833.9 eV). Fig. 3a shows the Co 2p core-level spectra of the products. LC-1 and LC-1.5 exhibits a Co $2p_{3/2}$ peak at a binding energy of 779 eV, lower than the one typically reported.[27] In addition, the absence of shake-up peaks in the spectra indicates the $LaCoO_3$ phase. The Co 2p profiles of LC-2, LC-3 and LC-5 derived from $LaCoO_3$ display satellite lines around 790 eV which is the fingerprint of Co_3O_4 species. Fig. 3b shows the O1s spectra of $LaCoO_3$. From the spectra, two kinds of oxygen species are observed with binding energies of 528.7-529.2 eV and 531.3-531.5 eV. These energies can be attributed to the surface lattice oxygen (O_{latt}) and the surface adsorbed oxygen (O_{ads}) species. [28-29] The O_{ads}/O_{latt} molar ratios are irregular for the untreated samples because of the impurities of La_2O_3 and Co_3O_4.

Fig. 3(c-d) shows the Mn $2p_{3/2}$ and O 1s XPS spectra of the $LaMnO_3$, respectively. There are Mn^{4+} and Mn^{3+} species as well as O_{latt} and O_{ads} species on the surfaces of $LaMnO_3$.[30-31] The surface atomic ratios of Mn^{4+}/Mn^{3+} and O_{ads}/O_{latt} have an important impact on the catalytic performance of $LaMnO_3$. The ratios of O_{ads}/O_{latt} of LM-1, LM-2, LM-3, LM-4, LM-5 and LM-6 are 0.21, 0.37, 0.48, 1.13, 1.39 and 1.02, respectively. LM-5 shows the highest O_{ads}/O_{latt} ratio. The ratios of Mn^{4+}/Mn^{3+} of LM-1, LM-2, LM-3, LM-4, LM-5 and LM-6 are 0.39, 0.32, 0.54, 0.57, 0.53 and 0.51, respectively. It is found that the surface atomic ratios of lanthanum and manganese of LM-5 is lower than 1, suggesting the presence of Mn enrichment on the surfaces of the samples. Such phenomena are also reported by other literature.[32] The differences in surface atomic ratio of Mn^{4+}/Mn^{3+} of $LaMnO_3$ samples is due to the different reactant ratio of lanthanum and manganese. [33]

Fig. 4a shows the H_2-TPR profiles of the as-prepared $LaCoO_3$. It can be observed that for LC-1 and LC-1.5, there are two major signals with shoulders in all products, which correspond to two consecutive reduction steps. These two steps have been previously discussed in the literatures.[34-35] The low-temperature peak is associated to the first reduction step of Co^{3+} to Co^{2+}. Whereas the second reduction step at high temperature is ascribed to the irreversible reduction of Co^{2+} in the oxygen deficient perovskite to Co^0. For LC-2, LC-3 and LC-5, the reduction peaks are observed at lower temperatures, which are attributed to the reduction of the absorbed oxygen and Co_3O_4.

Fig. 4b shows the H_2-TPR profiles of $LaMnO_3$. $LaMnO_3$ also exhibit stepwise reduction. $LaMnO_3$ show a low temperature reduction peak at 300 °C with a shoulder at 400 °C. The reduction peak at 300 °C is due to the reduction of Mn^{4+} to Mn^{3+} and the removal of non-stoichiometric oxygen and adsorbed oxygen species.[36] The shoulder at 300 °C is due to the single-electron reduction of unsaturated coordination Mn^{3+}, whereas the reduction peak above 650 °C is due to the reduction of the remaining Mn^{3+}.[37] The two reduction temperatures (400 °C and 750 °C) of the LM-1 sample are higher and sharper than those of other $LaMnO_3$ samples. When the ratio of lanthanum and manganese is 1:1, there is less Mn^{4+} in sample which shows a less H_2 consumption. With the increase of the ratio, the two reduction temperatures shift to lower temperature. LM-5 shows the excellent low-temperature reducibility (320 °C and 690 °C). In addition, the reduction peaks of LM-6 are observed at lower temperatures which are attributed to the reduction of absorbed oxygen and MnO_2.

In order to remove the Co_3O_4 and La_2O_3 from $LaCoO_3$, acetic acid was used to dissolve these impurities. Fig. S5 shows the XRD patterns of the acid washing $LaCoO_3$, and all of the samples are perovskite-type $LaCoO_3$ phase. No impure phases corresponding to lanthanum or cobalt oxides are detected. The EDX images of WLC-1, WLC-3 and WLC-5 are shown in Fig S6, which show the La/Co atom ratios of WLC-1, WLC-3 and WLC-5 are 1:1.04, 1:1.06 and 1:1.02, close to 1:1. The average crystal sizes decrease with increasing the amount of the impure oxides, which further results in the increase of specific surface area in Table 1. The small crystal size and large specific surface area are obtained when the content of Co_3O_4 increased. Similar phenomena were also observed in the preparation of ZrO_2 and SnO_2 nanoparticles.[38-39] The existence of Co_3O_4 can prevent the growth of $LaCoO_3$ nanocrystals.

After washing, XPS has been used to investigate the surface element compositions and metal oxidation states. Fig. S7 and Fig. 5(a-b) are the XPS spectra of the acid-treated $LaCoO_3$ samples. In Fig. S7, the samples of WLC-5, WLC-3, WLC-2, WLC-1, WLC-1.5 exhibited binding energies all around 833.9 eV, which implies the presence of species of La^{3+} only in $LaCoO_3$ (833.9 eV). These

results reveal La_2O_3 can be removed after acid washing, which is in agreement with XRD results (Fig. S5). Fig. 5a shows the Co 2p core levels for the acid-treated $LaCoO_3$. The spectra have $2p_{3/2}$ and $2p_{1/2}$ spin-orbit doublet peaks located at 780 and 796 eV, respectively. The absence of the satellite line around 786 and 790 eV which are the finger print of CoO and Co_3O_4, indicates that Co atoms in these samples are mainly in $LaCoO_3$ phase,[40] in accordance with the results of XRD. Fig. 5b illustrates the O 1s XPS spectra of the acid-treated $LaCoO_3$. The O_{ads}/O_{latt} ratios of WLC-1.5, WLC-2, WLC-3, WLC-5 of the samples after acid washing are 0.84, 1.23, 1.25, 1.95, 2.41, indicated that the high specific surface area could significantly enhance the adsorption capability of oxygen.

Fig. 6 shows the H_2-TPR profiles of the acid-treated $LaCoO_3$. The temperature of the low-temperature peak (Co^{3+} to Co^{2+}) of WLC-1.5 is 460 °C. The corresponding TPR peaks shift to a lower temperatures of 428 °C for WLC-1, 414 °C for WLC-2, 410 °C for WLC-3 and 324 °C for WLC-5. The high-temperature peaks (Co^{2+} to Co^0) also shift to a lower temperature. The positions of the reduction peaks are influenced by crystallite size,[41] which suggests that the decrease in average crystallite size and increase in specific surface area can enhance the reducibility of Co^{3+} to Co^{2+} and Co^{2+} to Co^0.

3.2. Catalytic activity of $LaMO_3$ (M=Co, Mn) hollow spheres

Fig. 7a and 7b show the methane combustion activity of the as-prepared $LaCoO_3$ and $LaMnO_3$. The catalytic activity is expressed in terms of the temperatures corresponding to 50% conversion (T_{50}) and 90% conversion (T_{90}) of methane. The values of T_{50} and T_{90} of the catalysts are listed in Table 2. In Fig. 7a, activity towards methane combustion increased significantly with increasing content of Co_3O_4. LC-5 displays the highest activity with a $T_{50\%}$ of 485 °C due to the highest content of Co_3O_4. Fig. 7b shows the catalytic activities of the as-prepared $LaMnO_3$. Table 2 shows the catalytic performance of the as-prepared $LaMnO_3$ samples. Among these samples, LM-5 exhibits the best activity and the $T_{50\%}$ and $T_{90\%}$ are 480 and 570 °C. When the La or Mn is excess in LM-1, LM-2, LM-3, LM-4 or LM-6, the catalytic activity of them are not good. Interestingly, when the La/Mn atom ratio is 1:1.07 in LM-5, the activity for methane combustion is the best due to its high specific surface area.

For the catalytic activities of the acid-treated $LaCoO_3$ (Fig. 8), the catalytic activities of WLC-1.5, WLC-1, WLC-2, WLC-3 and WLC-5 are gradually enhanced with the increase of specific surface area. The catalytic activity of WLC-5 ($T_{50\%}$=479 °C) are much better than other $LaCoO_3$ because the smallest crystallite size (11.6 nm), highest pore volume (0.157 cm^3/g), average pore size (79.8 nm) and specific surface area (37.9 m^2/g). The XPS and H_2-TPR results indicate WLC-5 has the highest ratio of O_{ads}/O_{latt} and the lowest reduction temperature. Sun's report also illustrated high specific surface area, adsorbed oxygen content and good reducibility helped to improve the catalytic activity. [42]

The different activities are likely related to the difference of the specific surface area. According to the activity data and the mole number of cobalt or manganese in samples, the turnover frequencies (TOFs) are calculated, and the results are shown in Table 2. It can be observed that WLC-5 (12.31×10^{-2} $mol_{CH4}/(mol_{Co}s)$) and LM-5 (11.43×10^{-2} $mol_{CH4}/(mol_{Mn}s)$) show the highest TOF value in $LaCoO_3$ or $LaMnO_3$ under the temperature of 400 °C. Compared with the other catalysts in Table 3, WLC-5 and LM-5 shows the lower $T_{50\%}$ and higher reaction rate.

Thermal durability of LC-5, WLC-5 and LM-5 were investigated, and the results are shown in Fig. 9. It is seen that the catalytic activity of WLC-5 and LM-5 are stable during 70 h test, with methane conversion keeping at around 99.2 % in WLC-5 and 99.4 % in LM-5 at the reaction temperature of 650 °C. Compared to WLC-5 and LM-5, LC-5 has the poor thermal durability. The methane conversion of LC-5 decrease after 30 h. This phenomenon may be the result of the small quantities of Co_3O_4 in LC-5, whose catalyst activity will decrease rapidly at high temperature or in the atmosphere with excessive water vapor. These experimental results indicate that the perovskite-type metal oxides are much more resistant to deactivation than the traditional noble-metal-based catalysts.

Different SO_2 poisoning behaviors over perovskites in methane oxidation were reported.[51-54] Exposed to 20 ppm of SO_2 for 15 h at 550 °C, a loss of 50 % and 90 % of the initial activity was observed for $LaMnO_3$ and $LaCoO_3$, respectively.[51] In our experiments, the sample of WLC-5 was exposed to 100 ppm of SO_2 at 600 °C for 3 h. Fig. S8a shows the catalytic activity of WLC-5 before and after SO_2 poisoning. The lost catalytic activity can be observed. T50 of the catalyst increases from 478 °C to 545 °C, and T_{90} increases from 582 °C to 640 °C, which reveal a loss of 20 % of the initial activity. Fig. S8b is the FTIR spectrum of the catalyst after SO_2 poisoned. The peaks at 1064 cm^{-1}, 1128 cm^{-1}, 1190 cm^{-1} indicate the formation of sulfate, which indicate the destruction of the perovskite structure. This destruction is considered the main reason leading to the deactivation of the perovskite catalyst.

4. Conclusions

In summary, high specific surface area $LaMO_3$ (M=Co, Mn) hollow spheres were synthesized by carbon sphere template method. High specific surface area, pore volume, pore size, ratio of O_{ads}/O_{latt}, and small crystallite size, good low-temperature reducibility were responsible for the excellent catalytic performance of $LaMO_3$ (M=Co, Mn) hollow sphere in methane combustion. We believe that this method has promising application in the synthesis of other perovskites.

The authors acknowledge the financial support from the China National Natural Science Funds (No. 21275016, 21105003, 20901008).

Notes and references

State Key Laboratory of Chemical Resource Engineering, Beijing University of Chemical Technology, Beijing, 100029, China. Tel: +86 10 64445927; E-mail: gufb@mail.buct.edu.cn, zhwang@mail.buct.edu.cn

† Electronic Supplementary Information (ESI) available: Fig. S1-Fig.S8. See DOI: 10.1039/b000000x/

1 D. Y. Liu and T. L. Kelly, *Nature Photonics*, 2014, **8**, 133-138.
2 X. W. Zhou, N. Yan, K. T. Chuang and J. K. Luo, *RSC Adv.*, 2014, **4**, 118-131.
3 P. Liu, J. Nisar, B. S. Sa, B. Pathak and R. Ahuja, *J. Phys. Chem. C*, 2013, **117**, 13845-13852.
4 H. Najjar and H. Batis, *Appl. Catal. A*, 2010, **383**, 192-201.
5 J. J. Kingsley and L. R. Pederson, *Mater. Lett.*, 1993, **18**, 89-96.

6 S. Cimino, R. Pirone, L. Lisi, M. Turco and G. Russo, *Catal. Today*, 2000, **59**, 19-31.
7 W. Yang, R. D. Zhang, B. H. Chen, D. Duprez and S. Royer, *Environ. Sci. Technol.*, 2012, **46**, 11280-11288.
8 H. Taguchi, D. Matsuda, M. Nagao, K. Tanihata and Y. Miyamoto, *J. Am. Ceram. Soc.*, 1992, **75**, 201-202.
9 H. Taguchi, H. Yoshioka, D. Matsuda and M. Nagao, *J. Solid State Chem.*, 1993, **104**, 460-463.
10 Y.C. Wei, J. Liu, Z. Zhao, Y. S. Chen, C. M. Xu, A. J. Duan, G. Y. Jiang and H. He, *Angew. Chem. Int. Ed.*, 2011, **50**, 2326-2329.
11 J. F. Xu, J. Liu, Z. Zhao, J. X. Zheng, G. Z. Zhang, A. J. Duan and G. Y. Jiang, *Catal. Today*, 2010, **153**, 136-142.
12 T. Zhang, F. B. Gu, D. M. Han, Z. H. Wang and G. S. Guo, *Sensor Actuat. B*, 2013, **177**, 1180-1188.
13 M. M. Titirici, M. Antonietti and A. Thomas, *Chem. Mater.* 2006, **18**, 3808-3812.
14 W. H. Shen, Y. F. Zhu, X. P. Dong, J. L. Gu and J. L. Shi, *Chem. Lett.*, 2005, **34**, 840-841.
15 X. L. Li, T. J. Lou, X. M. Sun and Y. D. Li, *Inorg. Chem.*, 2004, **43**, 5442-5449.
16 H. Y. Wang, R. J. Wang, X. M. Sun, R. X. Yan and Y. D. Li, *Mater. Res. Bull.*, 2005, **40**, 911-919.
17 S. Su, R. Z. Zuo, D. Z. Lv and J. Fu, *Powder Technol.*, 2012, **217**, 11-15.
18 B. R. Sneha and V. Thangadurai, *J. Solid State Chem.*, 2007, **180**, 2661-2669.
19 K. Eguchi and H. Arai, *Catal. Today*, 1996, **29**, 379-386.
20 X. M. Sun and Y. D. Li, *Angew. Chem. Int. Ed.*, 2004, **43**, 597-601.
21 X. M. Sun and Y. D. Li, *Angew. Chem. Int. Ed.*, 2004, **43**, 3827-3831.
22 Z. Dong, X. Lai, J. Halpert, N. Yang, L. Yi, J. Zhai, D. Wang, Z. Tang and L. Jiang, *Adv. Mater.*, 2012, **24**, 1046-1049.
23 H. Najjar, J. F. Lamonier, O. Mentre´, J. M. Giraudon and H. Batis, *Catal. Sci. Technol.*, 2013, **3**, 1002-1016
24 Z. Sarshar, F. Kleitzb and S. Kaliaguine, *Energy Environ. Sci.*, 2011, **4**, 4258-4269.
25 J. A. Villoria, M. C. Alvarez-Galvana, S. M. Al-Zahranib and P. Palmisanoc, *Appl. Catal. B*, 2011, **105**, 276-288.
26 Z. Guo, Z. W. Jiang, X. Chen, B. Sun, M. Q. Li, J. H. Liu and X. J. Huang, *J. Mater. Chem.*, 2011, **21**, 1874-1879.
27 L. G. Tejuca, J. L. G. Fierro and J. M. D. Tascon, *Adv. Catal.*, 1989, **36**, 237-328.
28 R. Lago, G. Bini, M. A. Pena and J. L. G. Fierro, *J. Catal.*, 1997, **167**, 198-209.
29 E. J. Crumlin, E. Mutoro, Z. Liu, M. E. Grass, M. D. Biegalski, Y. L. Lee, D.Morgan, H. M. Christen, H. Bluhm and Y. Shao-Horn, *Energy Environ. Sci.*, 2012, **5**, 6081-6088.
30 H. B. Deng, L. Lin, Y. Sun, C. S. Pang, J. P. Zhuang, P. K. Ouyang, Z. J. Li and S. J. Liu, *Catal. Lett.*, 2008, **126**, 106-111.
31 R. Horn, K. Williams, N. Degenstein, A. Bitsch-Larsen, D. DalleNogare, S. Tupy and L. Schmidt, *J. Catal.*, 2007, **249**, 380-393.
32 A. Machocki, T. Ioannides, B. Stasinska, W. Gac, G. Avgouropoulos, D. Delimaris, W. Grzegorczyk and S. Pasieczna, *J. Catal.*, 2004, **227**, 282-296.
33 Z. M. Li, X. Y. Lai, H. Wang, D. Mao, C. J. Xing and D. Wang, *J. Phys. Chem. C*, 2009, **113**, 2792-2797.
34 S. Royer, F. Beırubei and S. Kaliaguine, *Appl. Catal. A*, 2005, **282**, 273-277.
35 B. Levasseur and S. Kaliaguine, *Appl. Catal. B*, 2009, **88**, 305-314.
36 Y. J. Zhu, Y. Q. Sun, X. Y. Niu, F. L. Yuan and H. G. Fu, *Catal. Lett.*, 2010, **135**, 152-158.
37 F. Teng, W. Han, S. H. Liang, B. Gaugeu, R. L. Zong and Y. F. Zhu, *J. Catal.*, 2007, **250**, 1-11.
38 G. Pang, S. Chen, Y. Koltypin, A. Zaban, S. Feng and A. Gedanken, *Nano Lett.*, 2001, **1**, 723-276.
39 G. Pang, S. Chen, Y. Zhu, O. Palchik, Y. Koltypin, A. Zaban and A. Gedanken, *J. Phys. Chem. B*, 2001, **105**, 4647-4652.
40 H. M. Ismail, D. A. Cadenhead and M. I. Zaki, *J. Colloid Interf. Sci.*, 1997, **194**, 482-488.
41 L. Huang, M. Bassir and S. Kaliaguine, *Appl. Surface Sci.*, 2005, **243**, 360-375.
42 S. M. Sun, L. Yang, G. S. Pang and S. H. Feng, *Appl. Catal. A*, 2011, **401**, 199-203.
43 S. Cimino, S. Colonna, S. D. Rossi, M. Faticanti, L. Lisi, I. Pettiti and P. Porta, *J. Catal.*, 2002, **205**, 309-317.
44 H. Najjar, J. F. Lamonier, O. Mentré, J. M. Giraudon and H. Batis, *Appl. Catal. B*, 2011, **106**, 149-159.
45 X. Wei, P. Hug, R. Figi, M. Trottmann, A. Weidenkaff and D. Ferri, Appl. Catal. B, 2010, **94**, 27-37.
46 S. H. Liang, F. Teng, G. Bulgan and Y. F. Zhu, *J. Phys. Chem. C*, 2007, **111**, 16742-14749.
47 H. Taguchi, K. Matsu-ura, M. Takada and K. Hirota, *J. Solid State Chem.*, 2012, **190**, 157-161.
48 Y. Lu, A. Eyssler, E. Otal, S. K. Matam, O. Brunko, A. Weidenkaff and D. Ferri, *Catal. Today*, 2013, **208**, 42-47.
49 X. J. Zhang, Y. Li, H. J. Li and W. J. Shen, *J. Nat. Gas Chem.*, 2012, **21**, 113-118.
50 S. Specchia, F. Conti and V. Specchia, *Ind. Eng. Chem. Res.*, 2010, **49**, 11101-11111.
51 M. Alifanti, R. Auer, J. Kirchnerova, F. Thyrion, P. Grange and B. Delmon, *Appl. Catal. B*, 2003, **41**, 71-82.
52 M. J. Koponen, T. Venäläinen, M. Suvanto, K. Kallinen, T. J. J. Kinnunen, M. Härkönen and T. A. Pakkanen, *J. Mol. Catal. A*, 2006, **258**, 246-250.
53 O. Buchneva, I. Rossetti, C. Oliva, M. Scavini, S. Cappelli, B. Sironi, M. Allieta, A. Kryukovb and L. Fornia, *J. Mater. Chem.*, 2010, **20**, 10021-10031.
54 D. Trong On, S. V. Nguyena and S. Kaliaguine, *Phys. Chem. Chem. Phys.*, 2003, **5**, 2724-2729.

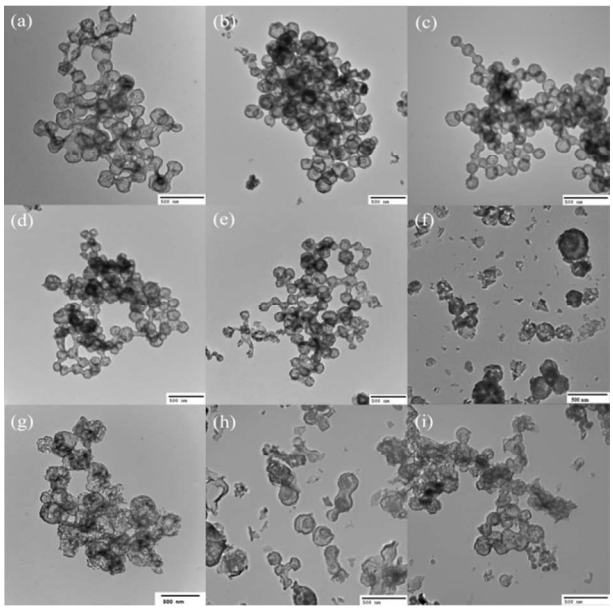

Fig.1 TEM images of $LaCoO_3$ hollow spheres: (a) LC-1, (b) LC-1.5, (c) LC-2, (d) LC-3, (e) LC-5 and $LaMnO_3$ hollow spheres: (f) LM-3, (g) LM-4, (h) LM-5, (i) LM-6.

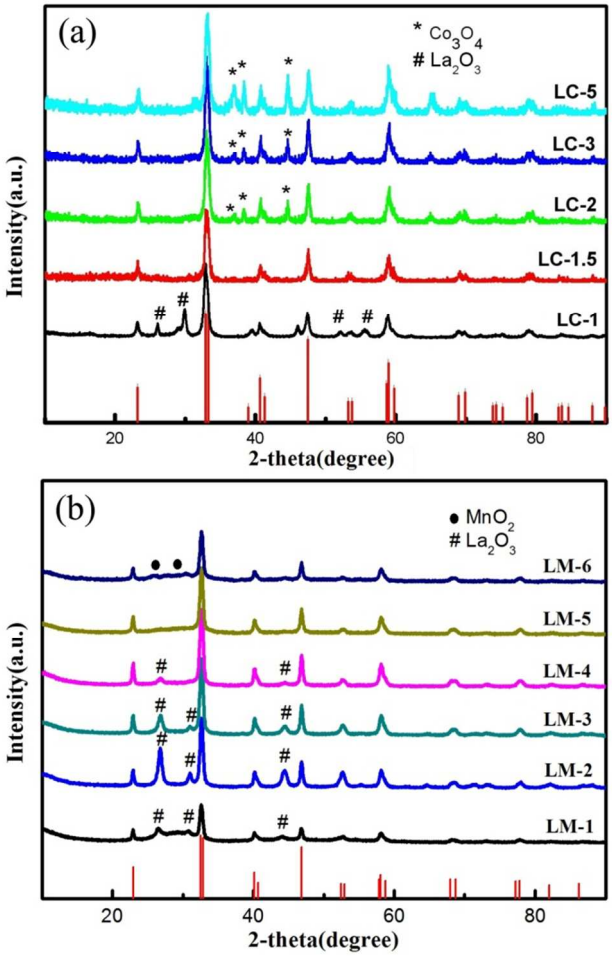

Fig.2 XRD patterns of $LaCoO_3$ (a) and $LaMnO_3$ (b) hollow spheres.

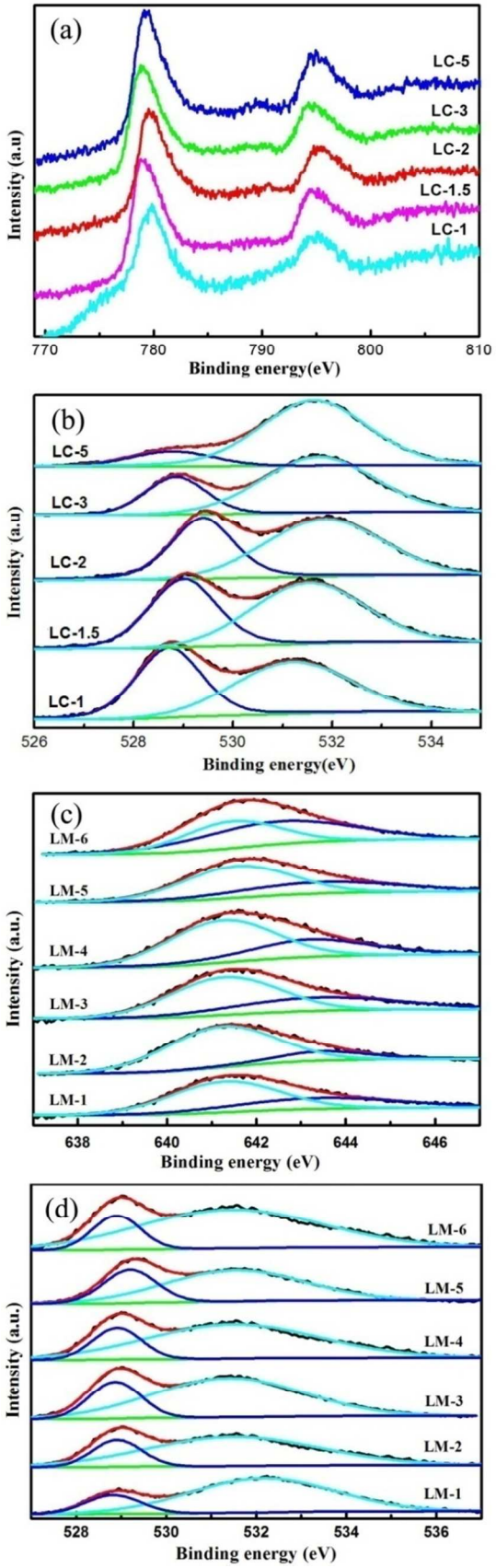

Fig.3 XPS spectra of the as-prepared $LaCoO_3$ of Co2p (a), O1s (b) and $LaMnO_3$ of Mn 2p3/2(c), O1s (d).

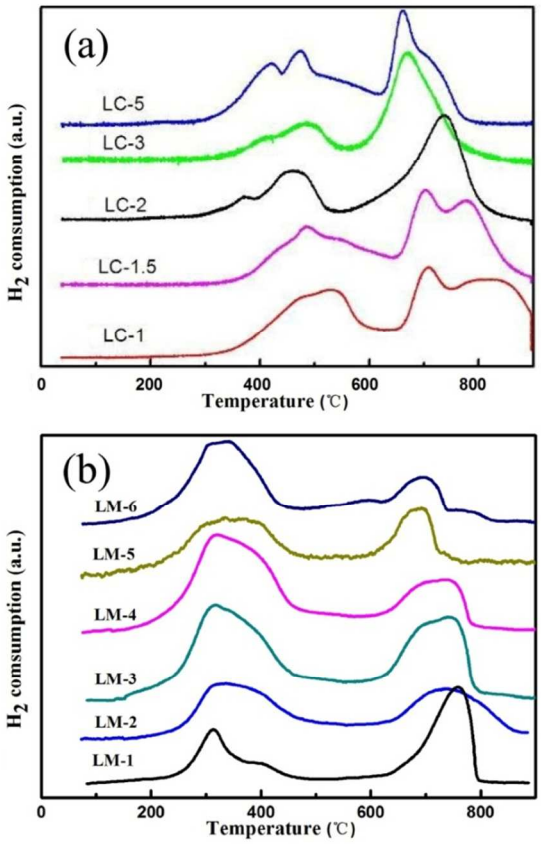

Fig.4 H_2-TPR profiles of the as-prepared $LaCoO_3$ (a) and $LaMnO_3$ (b).

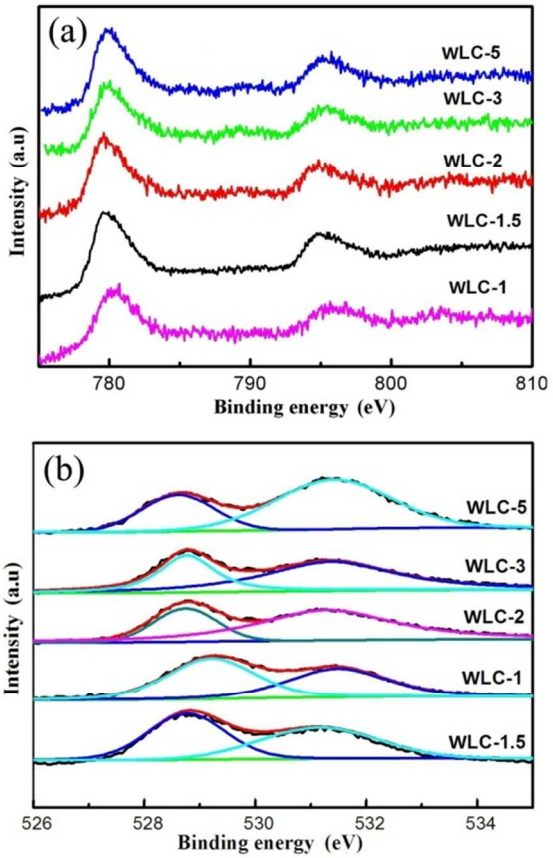

Fig.5 XPS spectra of the acid-treated $LaCoO_3$ of Co2p (a), O1s (b).

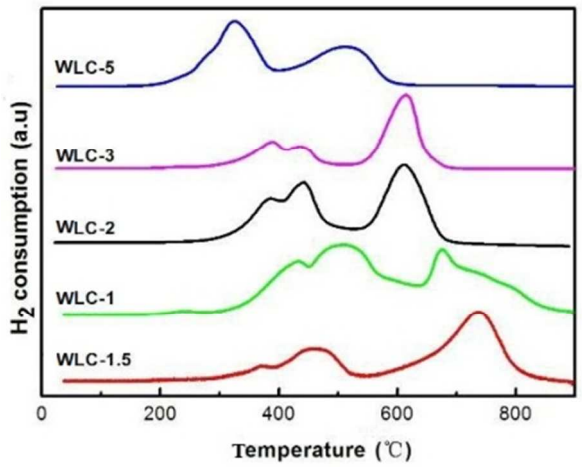

Fig.6 H_2-TPR profiles of the acid-treated $LaCoO_3$.

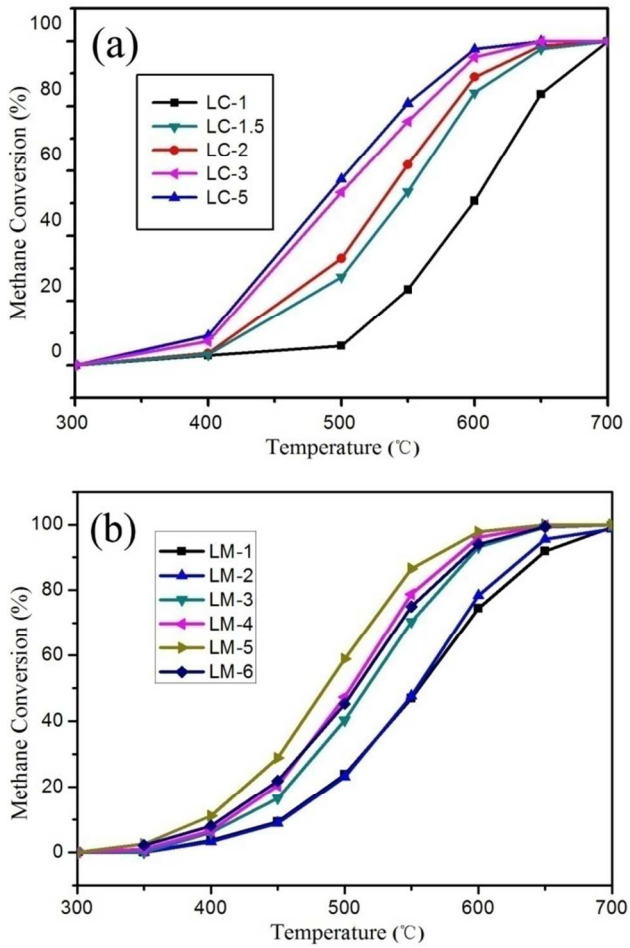

Fig.7 CH_4 oxidation as a function of temperature with $LaCoO_3$ (a) and $LaMnO_3$ (b).

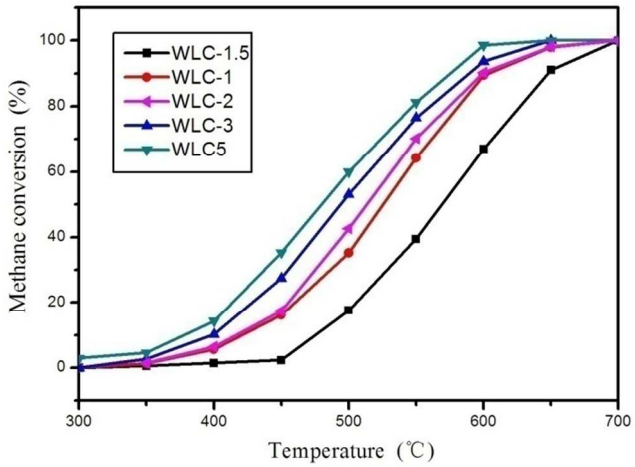

Fig.8 CH_4 oxidation as a function of temperature with the acid-treated $LaCoO_3$.

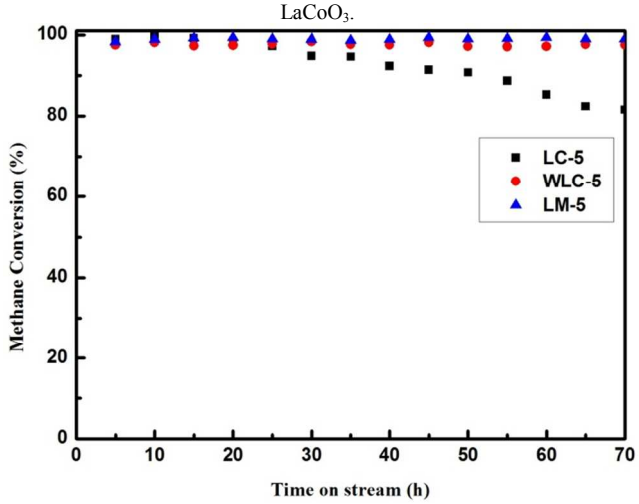

Fig.9 Methane conversion versus time at the reaction temperature of 650 °C of LC-5, WLC-5 and LM-5.

Table 1 List of crystallite sizes, specific surface areas, average pore sizes and pore volumes of $LaMO_3$ (M=Co, Mn).

Catalyst code	Crystallite size (nm)	Specific surface area (m^2/g)	Average pore size (nm)	Pore volume (cm^3/g)
LC-1.5	18.2	12.3	55.2	0.036
LC-1	19.0	13.0	61.7	0.042
LC-2	17.8	15.5	69.2	0.068
LC-3	16.4	18.6	65.3	0.075
LC-5	16.2	21.2	72.1	0.085
LM-1	17.2	23.0	55.9	0.064
LM-2	16.7	22.4	67.7	0.074
LM-3	16.4	27.9	70.7	0.098
LM-4	16.4	34.4	75.7	0.130
LM-5	16.8	42.6	75.4	0.153
LM-6	17.1	33.5	86.8	0.146
WLC-1.5	17.7	17.2	70.3	0.088
WLC-1	15.8	20.4	68.6	0.102
WLC-2	15.9	24.9	71.9	0.090
WLC-3	14.2	28.9	72.5	0.124
WLC-5	11.6	37.9	79.8	0.157

Table 2 List of reaction rate, TOF and the temperatures of T_{50} and T_{90} of $LaMO_3$ (M=Co, Mn).

Catalyst	Temperature (◦C)		Reaction rate ($\times10^{-3}$mmol $g^{-1}s^{-1}$)	TOF(mol_{CH4}/(mol_Ms) (M= Co or Mn)
	T_{50}	T_{90}	400 °C	400°C
LC-1	599	667	0.222	2.58×10^{-2}
LC-1.5	544	623	0.318	2.83×10^{-2}
LC-2	530	605	0.448	3.19×10^{-2}
LC-3	493	588	0.841	6.38×10^{-2}
LC-5	485	578	1.04	7.96×10^{-2}
LM-1	558	647	0.358	2.15×10^{-2}
LM-2	545	628	0.414	2.84×10^{-2}
LM-3	532	594	0.683	3.53×10^{-2}
LM-4	513	580	0.750	5.17×10^{-2}
LM-5	480	570	1.24	11.43×10^{-2}
LM-6	507	582	0.907	7.68×10^{-2}
WLC-1	525	605	0.640	4.82×10^{-2}
WLC-1.5	570	648	0.299	1.08×10^{-2}
WLC-2	513	599	0.744	5.48×10^{-2}
WLC-3	495	589	1.15	9.48×10^{-2}
WLC-5	479	576	1.61	12.31×10^{-2}

Table 3 List of specific surface area, the temperatures corresponding to T_{50}, T_{90} and reaction rate ($\times10^{-7}$ mol_{CH4} $g^{-1}s^{-1}$) of the different catalysts in the literature.

Catalysts	Specific surface area (m^2/g)	T_{50}	T_{90}	Reaction rate ($\times10^{-7}mol_{CH4}$ $g^{-1}s^{-1}$)[a]	Reference
$LaMnO_3$	15	511	599	1.39	43
$LaMnO_3$	37	521	612	2.98	44
$LaCoO_3$	5.5	560	640	0.94	45
$La_{0.5}Sr_{0.5}MnO_3$	9.3	524	575	9.28	46
$La_{0.96}Ca_{0.04}CoO_3$	4.3	541	623	0.67	47
$La(Mn,Pd)O_3$	12	495	586	4.46	48
$LaFe_{0.95}Pd_{0.05}O_3$	5.2	554	638	0.89	49
$Ce_xZr_{1-x}O_2$	16.5	580	680	1.86	50
WLC-5	37.9	479	576	16.1	this work
LM-5	42.6	480	570	12.4	this work

[a] at 400 °C